ELSEVIER

International Journal of Solids and Structures 41 (2004) 4503–4516

INTERNATIONAL JOURNAL OF SOLIDS and STRUCTURES

www.elsevier.com/locate/ijsolstr

Bistable composite slit tubes. II. A shell model

Diana A. Galletly, Simon D. Guest *

Department of Engineering, University of Cambridge, Trumpington Street, Cambridge CB2 1PZ, UK

Received 23 September 2003; received in revised form 13 February 2004
Available online 15 April 2004

Abstract

The detailed shape of bistable tubes at a second stable equilibrium point is examined. The existence of a short 'boundary layer' at the edge of the tube is found, which is particularly significant for tubes that are initially shallow.

Keywords: Bistable; Composite

1. Introduction

The first paper of this series, Part I (Galletly and Guest, 2004), presented a *beam model* to describe the behaviour of a novel structure, the *bistable composite slit tube*. These tubes have an initial state as thin-walled ribs with a cross-section that is a circular arc. For certain composite layups, these tube have a second, coiled, stable configuration.

The beam model for the tubes assumed that the cross-section of the structure remained as an arc of a circle, with a radius that was allowed to vary. This paper presents a new model, the *shell model*, which does not make any assumption about the cross-sectional shape. Instead a differential equation is set up to model the transverse shape, and this is used to find a second equilibrium configuration. The model again assumes that the tube is longitudinally uniform, and is hence not trying to model the transition from the rolled to the extended state, which takes place in a small transition zone, but is trying to discover the detailed shape at a possible second equilibrium configuration.

The paper is structured as follows. Section 2 sets up a differential equation for the transverse shape, which can be solved in terms of two unknowns, the longitudinal curvature ($1/a$), and the twist (Φ). The transverse shape, and both a and Φ, can then be found by ensuring that the structure is at an equilibrium point, and the stability of the equilibrium can be checked by calculating the tangent-stiffness matrix.

Section 3 uses the new shell model to investigate the same cases that were considered for the beam model in Part I: tubes made from symmetric and antisymmetric composite layups, and from an isotropic sheet.

* Corresponding author. Tel.: +44-1223-332708; fax: +44-1223-332662.
E-mail addresses: dag1000@eng.cam.ac.uk (D.A. Galletly), sdg@eng.cam.ac.uk (S.D. Guest).

0020-7683/$ - see front matter © 2004 Elsevier Ltd. All rights reserved.
doi:10.1016/j.ijsolstr.2004.02.037

We compare the transverse shape found using the shell model with the constant transverse curvature assumption of the beam model, and discuss the validity of this assumption.

Section 4 compares the results of the shell model with previous experimental and computational results, and in particular compares the cross-sectional shape predicted at a second equilibrium.

Section 5 concludes the paper.

2. Derivation of model

The following calculation for the transverse shape is based on Calladine's derivation of the shape of an isotropic cylinder due to an edge load (Calladine, 1983, Chapter 3). Here we present a similar derivation, but for a more general, composite case that also allows the possibility that the structure may *twist*. A basic assumption is that the tube remains longitudinally uniform, and hence we only have to consider a representative section.

The derivation proceeds as follows: initially the tube is transformed from the extended state to a coiled state with a uniform radius, a, and no circumferential strain ϵ_x, as shown in Fig. 1(a). It is straightforward to show that this configuration cannot satisfy the no-transverse moment condition at $y = \pm l/2$, and hence we allow each point on the cross-section to displace outwards by $w(y)$, so that a longitudinal strand that formed a circle of radius a becomes a circle of radius $a + w(y)$, as shown in Fig. 1(b). We then also assume that the tube is allowed to twist uniformly by a twist/unit length Φ (equivalent to Φ_X in Part I), so that the tube takes up a general helical configuration.

Following Calladine, we define in Section 2.1 two differential equilibrium equations, by resolving out-of-plane forces, and transverse moments. Combining these equations gives a governing fourth-order differential equation for $w(y)$.

A general solution for the governing equation is calculated in Section 2.2. Appropriate boundary conditions are applied, and $w(y)$, the transverse shape of the shell, is found in terms of two as-yet-unknown parameters, the initial coiled radius of curvature, a, and the twist, Φ. These parameters are found by

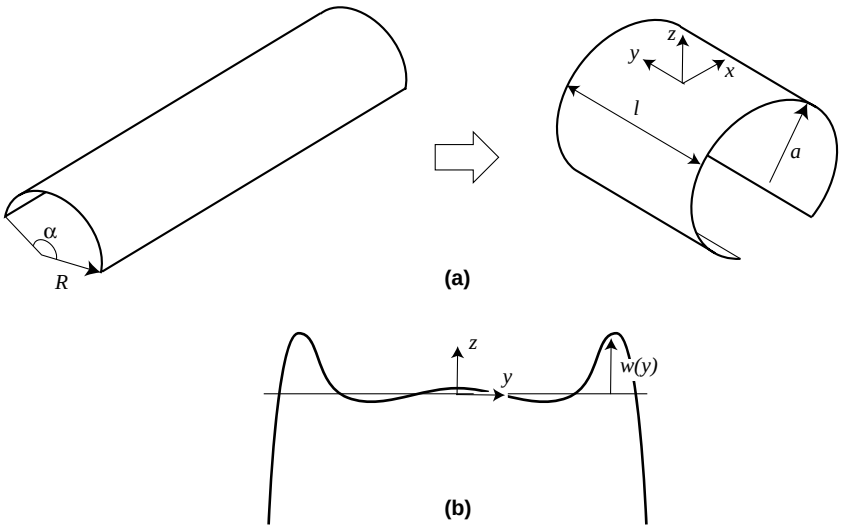

Fig. 1. Transformation of the tube from its initial to second equilibrium state: (a) initial coiling; (b) adjustment of the cross-sectional shape, not shown to scale—we assume that $w(y) \ll a$.

ensuring overall equilibrium, in Section 2.3. The tangent-stiffness matrix, for checking stability, is described in Section 2.4.

2.1. Calculating the cross-sectional shape

Fig. 2 shows the stress resultants acting on a small element of shell. In order to assist with setting up the equilibrium equations, the changes in the values of M_y and Q_y with y are shown. N_x is positive when tensile, and the bending moments M_x and M_y are positive when they produce tension on the positive z face of the shell. Q_y points in the positive z direction on the positive y face of the shell. M_{xy} is defined such that the shear stress τ_{xy}, is positive on the positive z face of the shell. The shell is considered to be uniform in the x-direction, and hence there is no variation in M_x and N_x with x, and thus $Q_x = 0$. N_y and N_{xy} must be zero on the edge of the shell, which is not loaded, and this derivation assumes that they are zero everywhere. There is no pressure loading applied to the shell.

2.1.1. Equilibrium equations

Two equilibrium equations are found, by resolving forces in the z-direction, and by taking moments about a longitudinal x-axis.

There are two transverse force components: the shear force imbalance, $(\mathrm{d}Q_y/\mathrm{d}y)\delta y\,\delta x$, and a component from the two N_x forces of $N_x(\delta x/a)\delta y$. Combining these components leads to the first equilibrium equation:

$$\frac{\mathrm{d}Q_y}{\mathrm{d}y} - \frac{N_x}{a} = 0. \tag{1}$$

Taking moments about an axis tangential to the element in the circumferential direction, for the limit, as $\mathrm{d}y$ tends to zero:

$$\frac{\mathrm{d}M_y}{\mathrm{d}y} - Q_y = 0. \tag{2}$$

Combining these two equilibrium equations by eliminating Q_y, gives

$$\frac{\mathrm{d}^2M_y}{\mathrm{d}y^2} - \frac{N_x}{a} = 0, \tag{3}$$

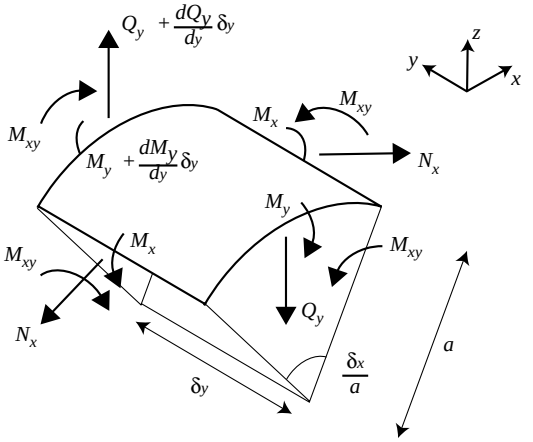

Fig. 2. Stress resultants acting on a small shell element. N_y and N_{xy} are taken to be zero, and are not shown.

M_y and N_x can be written in terms of $w(y)$, Φ, and a by considering kinematic compatibility, and the stress–strain law.

2.1.2. Stress–strain law

The reduced stress–strain relationship that we use for composite materials (derived for cases such as this one where $N_y = N_{xy} = 0$) was described in Part I. As in that paper, we shall assume, to simplify some of the algebra, that we are only considering symmetric or antisymmetric layups of composite, and hence $B^*_{11} = B^*_{12} = 0$. The remaining relationships then become

$$\begin{pmatrix} N_x \\ M_x \\ M_y \\ M_{xy} \end{pmatrix} = \begin{bmatrix} A^*_{11} & 0 & 0 & B^*_{16} \\ 0 & D^*_{11} & D^*_{12} & D^*_{16} \\ 0 & D^*_{12} & D^*_{22} & D^*_{26} \\ B^*_{16} & D^*_{16} & D^*_{26} & D^*_{66} \end{bmatrix} \begin{pmatrix} \epsilon_x \\ \kappa_x \\ \kappa_y \\ \kappa_{xy} \end{pmatrix}, \tag{4}$$

ϵ_x, κ_x, κ_y, and κ_{xy} are strains that are work-conjugate with N_x, M_x, M_y, and M_{xy}, respectively, and the starred terms are transformed material stiffnesses as described in Part I.

2.1.3. Compatibility equations

For the assumed shape shown in Fig. 1(b), we can find the strains, κ_y, κ_x, κ_{xy}, and ϵ_x, in the structure.

κ_y: In the undeformed state, the structure has a transverse curvature of $1/R$, and in the initially coiled shape, zero transverse curvature. As the cylinder deforms due to the displacement $w(y)$, a further change in curvature is induced. This curvature is given by $-\mathrm{d}^2w/\mathrm{d}y^2$, and thus

$$\kappa_y = -\frac{\mathrm{d}^2 w}{\mathrm{d}y^2} - \frac{1}{R}. \tag{5}$$

κ_x: In the undeformed state, the structure has zero circumferential curvature, and in its initially coiled state it has a circumferential curvature of $1/a$. After the displacement $w(y)$ the radius becomes $a + w(y)$, and hence the curvature is $1/a + w(y)$. However, we assume that $w(y) \ll a$, and hence

$$\kappa_x = \frac{1}{a}. \tag{6}$$

κ_{xy} is the twisting curvature, $-2\mathrm{d}^2w/\mathrm{d}x\,\mathrm{d}y$, and is equal to -2Φ, as described in Part I.

ϵ_x: Due to the displacement $w(y)$, each circumferential strand that had a radius a now has a radius $a + w(y)$. Thus, initially neglecting twisting, the strain due to the displacement w alone is given by

$$\epsilon_{xw} = \frac{w(y)}{a}. \tag{7}$$

The derivation of the twist-induced component of circumferential strain that causes no overall axial force, $\epsilon_{x\Phi}$, is given in Part I for a material where $B^*_{11} = B^*_{12} = 0$. Making the same assumption here,

$$\epsilon_{x\Phi} = \frac{\Phi^2}{2}\left[y^2 - \frac{l^2}{12}\right] + \frac{2B^*_{16}}{A^*_{11}}\Phi. \tag{8}$$

Summing the two components for circumferential strain gives

$$\epsilon_x = \frac{w(y)}{a} + \frac{\Phi^2}{2}\left[y^2 - \frac{l^2}{12}\right] + \frac{2B^*_{16}}{A^*_{11}}\Phi. \tag{9}$$

2.1.4. Governing equation

Substituting the expressions for strains, Eqs. (5)–(9), into the stress–strain law, Eq. (4), gives

$$N_x = A_{11}^*\left(\frac{w(y)}{a} + \frac{\Phi^2}{2}\left(y^2 - \frac{l^2}{12}\right)\right), \tag{10}$$

$$M_y = D_{22}^*\left(-\frac{\mathrm{d}^2 w}{\mathrm{d}y^2} - \frac{1}{R}\right) + D_{12}^*\left(\frac{1}{a}\right) - 2D_{26}^*\Phi. \tag{11}$$

By substituting Eqs. (10) and (11) into Eq. (3), the governing equation for $w(y)$ is found to be

$$D_{22}^*\left(-\frac{\mathrm{d}^4 w}{\mathrm{d}y^4}\right) - A_{11}^*\left(\frac{w(y)}{a^2} + \frac{\Phi^2}{2a}\left(y^2 - \frac{l^2}{12}\right)\right) = 0. \tag{12}$$

Which can be written as

$$\frac{\mathrm{d}^4 w}{\mathrm{d}y^4} + \frac{4}{\mu^4}w(y) = -a\left(\frac{4}{\mu^4}\right)\left(\frac{\Phi^2}{2}\left(y^2 - \frac{l^2}{12}\right)\right), \tag{13}$$

where

$$\mu = (2a)^{\frac{1}{2}}\left(\frac{D_{22}^*}{A_{11}^*}\right)^{\frac{1}{4}}, \tag{14}$$

μ has the dimensions of length, and for the isotropic case is the geometric mean of a, and the thickness of the shell.

Eq. (13) is an extension of the well-known 'beam-on-elastic-foundation' equation, as discussed by Calladine (1983). Calladine's derivation is for an isotropic shell which did not undergo any twist. Mansfield (1973) derived a similar equation for an isotropic material which was permitted to twist; Eq. (13) reduces to Mansfield's equation by the substitution of the terms of the isotropic reduced stiffness matrix given in Part I. Eckold (1994) derived a similar equation for a composite shell which did not undergo any twist. Eq. (13) reduces to Eckold's solution for $\Phi = 0$.

2.2. Solution for the transverse shape of the shell

We can calculate the general solution of Eq. (13) in the usual fashion (e.g., James, 1996):

$$w(y) = K_1 \sinh\frac{y}{\mu}\sin\frac{y}{\mu} + K_2\cosh\frac{y}{\mu}\sin\frac{y}{\mu} + K_3\sinh\frac{y}{\mu}\cos\frac{y}{\mu} + K_4\cosh\frac{y}{\mu}\cos\frac{y}{\mu} - \frac{a\Phi^2}{2}\left(y^2 - \frac{l^2}{12}\right). \tag{15}$$

Applying the boundary conditions that there are no applied shear forces or moments along the edges $y = \pm l/2$,

$$Q_y = 0 \;\Rightarrow\; \frac{\mathrm{d}M_y}{\mathrm{d}y} = 0 \;\Rightarrow\; \frac{\mathrm{d}^3 w}{\mathrm{d}y^3} = 0 \quad \text{at } y = \pm\frac{l}{2},$$

$$M_y = 0 \quad \text{at } y = \pm\frac{l}{2}.$$

Thus,

$$K_1 = -\frac{\mu^2}{2}\left[\frac{1}{R} - a\Phi^2 - \frac{D_{12}^*}{D_{22}^*}\left(\frac{1}{a}\right) + 2\frac{D_{26}^*}{D_{22}^*}\Phi\right]c_1,$$

$$K_2 = 0,$$

$$K_3 = 0,$$

$$K_4 = -\frac{\mu^2}{2}\left[\frac{1}{R} - a\Phi^2 - \frac{D^*_{12}}{D^*_{22}}\left(\frac{1}{a}\right) + 2\frac{D^*_{26}}{D^*_{22}}\Phi\right]c_4,$$

where

$$c_1 = \left[\frac{\sinh\frac{l}{2\mu}\cos\frac{l}{2\mu} + \cosh\frac{l}{2\mu}\sin\frac{l}{2\mu}}{\sinh\frac{l}{2\mu}\cosh\frac{l}{2\mu} + \sin\frac{l}{2\mu}\cos\frac{l}{2\mu}}\right], \qquad c_4 = \left[\frac{\sinh\frac{l}{2\mu}\cos\frac{l}{2\mu} - \cosh\frac{l}{2\mu}\sin\frac{l}{2\mu}}{\sinh\frac{l}{2\mu}\cosh\frac{l}{2\mu} + \sin\frac{l}{2\mu}\cos\frac{l}{2\mu}}\right].$$

Substituting into Eq. (15) gives an expression for $w(y)$, and hence the transverse shape of the shell, in terms of two unknown parameters, a and Φ:

$$w(y) = -\frac{\mu^2}{2}\left[\frac{1}{R} - a\Phi^2 - \frac{D^*_{12}}{D^*_{22}}\left(\frac{1}{a}\right) + 2\frac{D^*_{26}}{D^*_{22}}\Phi\right]\left(c_1\sinh\frac{y}{\mu}\sin\frac{y}{\mu} + c_4\cosh\frac{y}{\mu}\cos\frac{y}{\mu}\right) - \frac{a\Phi^2}{2}\left(y^2 - \frac{l^2}{12}\right). \tag{16}$$

We now need to find values of a and Φ such that the shell is in equilibrium.

2.3. The global forces associated with the solution

The global forces that are work-conjugate with the twist Φ, and the curvature $1/a$, are a torque, T, and a longitudinal moment, M_l. They can be found by virtual work.

Following the derivation in Part I gives

$$T = \int_{-\frac{l}{2}}^{\frac{l}{2}}\left(N_x\frac{\partial\epsilon_x}{\partial\Phi} + M_x\frac{\kappa_x}{\partial\Phi} + M_y\frac{\partial\kappa_y}{\partial\Phi} + M_{xy}\frac{\partial\kappa_{xy}}{\partial\Phi}\right)\mathrm{d}y. \tag{17}$$

After substituting the expressions for strains, Eqs. (5)–(9), and the stress–strain law, Eq. (4), some considerable algebraic manipulation gives

$$T = 2lD^*_{22}\left[a\Phi^2 + \frac{D^*_{12}}{D^*_{22}}\left(\frac{1}{a}\right) - 2\frac{D^*_{26}}{D^*_{22}}\Phi - \frac{1}{R}\right]\left[a\Phi - \frac{D^*_{26}}{D^*_{22}}\right]d_1 + 4l\Phi\left(-\frac{B^{*^2}_{16}}{A^*_{11}} + D^*_{66} - \frac{D^{*^2}_{26}}{D^*_{22}}\right) - \frac{2l}{a}\left(D^*_{16} - D^*_{26}\frac{D^*_{12}}{D^*_{22}}\right), \tag{18}$$

where,

$$d_1 = 1 - \frac{2\mu}{l}\left(\frac{\cosh\frac{l}{\mu} - \cos\frac{l}{\mu}}{\sinh\frac{l}{\mu} + \sin\frac{l}{\mu}}\right). \tag{19}$$

Similarly

$$M_l = \int_{-\frac{l}{2}}^{\frac{l}{2}}\left(N_x\frac{\partial\epsilon_x}{\partial\left(\frac{1}{a}\right)} + M_x\frac{\partial\kappa_x}{\partial\left(\frac{1}{a}\right)} + M_y\frac{\partial\kappa_y}{\partial\left(\frac{1}{a}\right)} + M_{xy}\frac{\partial\kappa_{xy}}{\partial\left(\frac{1}{a}\right)}\right)\mathrm{d}y, \tag{20}$$

which gives

$$M_l = -D_{22}^* la\left[a\Phi^2 + \frac{D_{12}^*}{D_{22}^*}\frac{1}{a} - 2\frac{D_{26}^*}{D_{22}^*}\Phi - \frac{1}{R}\right]^2 d_2 - D_{22}^* l\left[a\Phi^2 + \frac{D_{12}^*}{D_{22}^*}\frac{1}{a} - 2\frac{D_{26}^*}{D_{22}^*}\Phi - \frac{1}{R}\right]\left[\Phi^2 a^2 - \frac{D_{12}^*}{D_{22}^*}\right] d_1 - 2\left(D_{16}^* - \frac{D_{26}^* D_{12}^*}{D_{22}^*}\right) l\Phi + \left(D_{11}^* - \frac{D_{12}^{*2}}{D_{22}^*}\right)\left(\frac{l}{a}\right), \tag{21}$$

where d_1 is given by Eq. (19), and

$$d_2 = \frac{\sinh\frac{l}{\mu}\sin\frac{l}{\mu}}{\left(\sinh\frac{l}{\mu} + \sin\frac{l}{\mu}\right)^2} - \frac{\mu}{2l}\left(\frac{\cosh\frac{l}{\mu} - \cos\frac{l}{\mu}}{\sinh\frac{l}{\mu} + \sin\frac{l}{\mu}}\right). \tag{22}$$

Equilibrium configurations can be found by ensuring that $T = M_l = 0$.

2.4. Stability criteria

Finding values of a and Φ such that $T = M_l = 0$ give equilibrium configurations, but it is also necessary to check the stability of the equilibrium, by ensuring that the local tangent-stiffness matrix $[\mathbf{H}]$ is positive-definite, where

$$[\mathbf{H}] = \begin{bmatrix} \dfrac{\partial T}{\partial \Phi} & \dfrac{\partial M_l}{\partial \Phi} \\ \dfrac{\partial T}{\partial\left(\frac{1}{a}\right)} & \dfrac{\partial M_l}{\partial\left(\frac{1}{a}\right)} \end{bmatrix}. \tag{23}$$

Full expansions for $\partial T/\partial\Phi$ etc. are not given here due to their length, but they will be found in Galletly (2001).

3. Results

Results are presented for the same four sample cases that were investigated for the beam model in Part I: an antisymmetric $[+45°, -45°, 0°, +45°, -45°]$ layup; symmetric $[+45°, -45°, 0°, -45°, +45°]$ and $[+40°, -40°, 0°, -40°, +40°]$ layups, and an isotropic case. All the samples have an initial transverse radius of curvature $R = 29$ mm. For each case we show:

- simplified expressions for the torque and moments, taking into account the appropriate zero terms in the reduced stiffness matrix;
- the position (a and Φ) of equilibrium points for varying $\alpha = l/R$ (shown in Fig. 1), and whether these equilibria are stable;
- for any stable equilibria, a comparison with the results for a and Φ predicted by the beam model;
- for any stable equilibria, the shape of the transverse cross-section, compared with the constant transverse curvature assumption of the beam model.

3.1. Antisymmetric layup

For an antisymmetric layup, $D_{16}^* = D_{26}^* = 0$, and the expressions for the torque and the longitudinal moment reduce to

$$T = 2D_{22}^{*} la\Phi\left[a\Phi^2 + \frac{D_{12}^{*}}{D_{22}^{*}}\left(\frac{1}{a}\right) - \frac{1}{R}\right]d_1 + 4l\Phi\left(D_{66}^{*} - \frac{B_{16}^{*2}}{A_{11}^{*}}\right), \tag{24}$$

$$M_l = \left(D_{11}^{*} - \frac{D_{12}^{*2}}{D_{22}^{*}}\right)\left(\frac{l}{a}\right) - D_{22}^{*} l\left[a\Phi^2 + \frac{D_{12}^{*}}{D_{22}^{*}}\frac{1}{a} - \frac{1}{R}\right]\left[\Phi^2 a^2 - \frac{D_{12}^{*}}{D_{22}^{*}}\right]d_1 - D_{22}^{*} la\left[a\Phi^2 + \frac{D_{12}^{*}}{D_{22}^{*}}\frac{1}{a} - \frac{1}{R}\right]^2 d_2. \tag{25}$$

For the 45° layup, solving these equations numerically allows equilibrium points ($T = M_l = 0$) to be found for α greater than a critical value, which for this example is $\alpha \geqslant 60°$. Fig. 3 shows how the values of a and Φ at the second equilibrium point vary with the initial cross-sectional angle α. A number of different solutions are possible, but only one is stable. Fig. 4 shows a comparison of the stable results predicted by the beam and shell models. In both cases, for large α, the results tend towards $R/a = 0.752$ with $\Phi R = 0$.

Fig. 5 shows the transverse cross-sectional shape, $w(y)$, calculated for both the beam and the shell model, for three different values of α. For $\alpha = 360°$, the models are essentially in agreement, apart from a short 'boundary layer' that is predicted by the shell model to form at the edges of the section. This boundary layer remains approximately constant as α is changed. For small values of α, e.g. $\alpha = 90°$, the boundary layers essentially make up the full width of the tube. In this case, the beam model, with its assumption of constant cross-sectional curvature, gives quite different results, and it is clear that this assumption is not valid.

3.2. Symmetric layup

For a symmetric layup, $B_{16}^{*} = 0$, and the expressions for the torque and the longitudinal moment reduce to

$$T = 2lD_{22}^{*}\left[a\Phi^2 + \frac{D_{12}^{*}}{D_{22}^{*}}\left(\frac{1}{a}\right) - 2\frac{D_{26}^{*}}{D_{22}^{*}}\Phi - \frac{1}{R}\right]\left[a\Phi - \frac{D_{26}^{*}}{D_{22}^{*}}\right]d_1 + 4l\Phi\left(D_{66}^{*} - \frac{D_{26}^{*2}}{D_{22}^{*}}\right) - \frac{2l}{a}\left(D_{16}^{*} - \frac{D_{12}^{*}D_{26}^{*}}{D_{22}^{*}}\right), \tag{26}$$

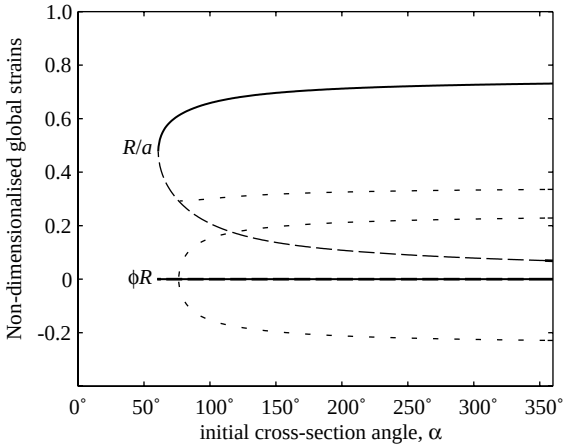

Fig. 3. Equilibrium points in addition to the initial state for the 45° antisymmetric layup. There is only one *stable* state, shown by the solid line, and this exists for $\alpha \geqslant 60°$. This solution has a corresponding unstable branch shown by the dashed line. At $\alpha = 76°$ a bifurcation leads to two twisted (one with positive twist, one with negative twist) unstable solutions, shown by dotted lines.

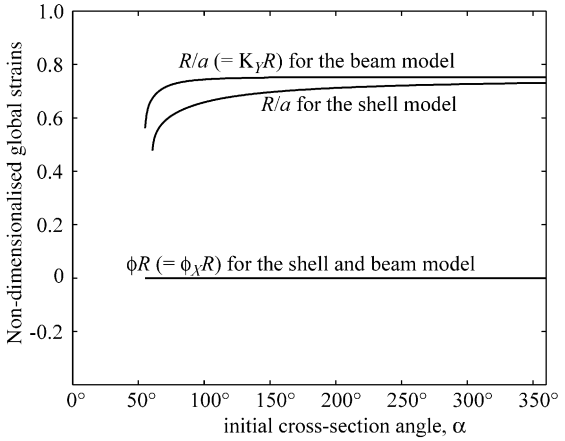

Fig. 4. A comparison of the prediction for the position of a second stable equilibrium configuration for the beam and shell models with a 45° antisymmetric layup.

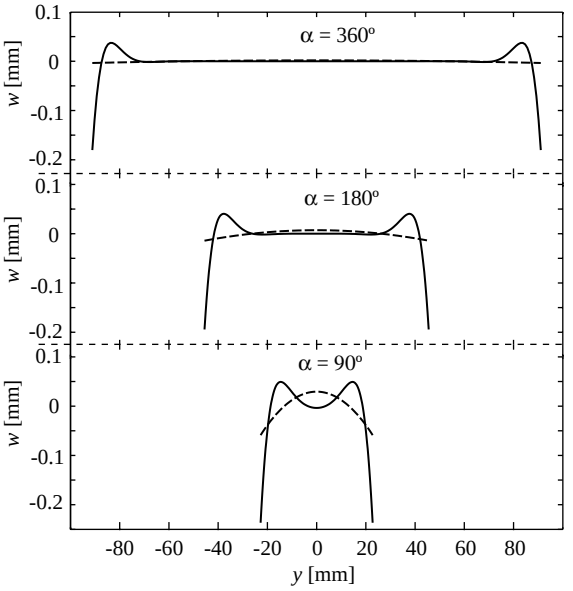

Fig. 5. Cross-sectional shape at the second stable equilibrium, for $\alpha = 90°$, 180°, and 360° for the 45° antisymmetric layup. The solid lines are the predictions made by the shell model. The dashed lines are the predictions made by the beam model. The vertical scale is magnified 200 times compared with the horizontal scale.

$$M_l = -2\left(D_{16}^* - \frac{D_{26}^* D_{12}^*}{D_{22}^*}\right) l\Phi + \left(D_{11}^* - \frac{D_{12}^{*2}}{D_{22}^*}\right)\left(\frac{l}{a}\right) - D_{22}^* l\left[\Phi^2 a^2 - \frac{D_{12}^*}{D_{22}^*}\right]\left[a\Phi^2 + \frac{D_{12}^*}{D_{22}^*}\left(\frac{1}{a}\right) - 2\frac{D_{26}^*}{D_{22}^*}\Phi - \frac{1}{R}\right] d_1$$
$$- D_{22}^* la\left[a\Phi^2 + \frac{D_{12}^*}{D_{22}^*}\left(\frac{1}{a}\right) - 2\frac{D_{26}^*}{D_{22}^*}\Phi - \frac{1}{R}\right]^2 d_2. \tag{27}$$

3.2.1. 45° layup

Solving Eqs. (26) and (27) numerically for a 45° layup shows that the only stable solution in addition to the original state exists only for very large α. In the range of practical interest, e.g. $\alpha \leqslant 360°$, there are *no* additional stable solutions; unstable twisted solutions appear for $\alpha \geqslant 165°$. Fig. 6 shows how the values of a and Φ for the unstable equilibria vary with the initial cross-sectional angle α.

3.2.2. 40° layup

Solving Eqs. (26) and (27) numerically for a 40° layup shows that there is a stable twisted solution, that appears for $\alpha \geqslant 202°$, in addition to the unstable solutions that are little altered from those presented in Fig. 6. Fig. 7 shows how the values of a and Φ at the equilibrium point vary with the initial cross-sectional angle

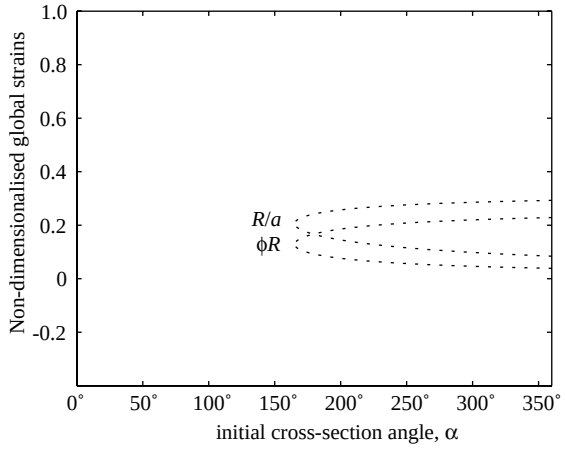

Fig. 6. Equilibrium points in addition to the initial state for the 45° symmetric layup. Unstable equilibria exist for $\alpha \geqslant 165°$, and are shown by dotted lines.

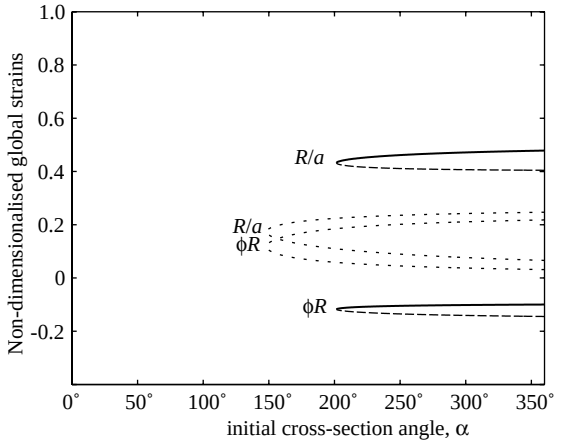

Fig. 7. Equilibrium points in addition to the initial state for the 40° symmetric layup. There is only one *stable* state, shown by the solid line, and this exists for $\alpha \geqslant 202°$. This solution has a corresponding unstable branch shown by the dashed line. Additional unstable solutions are shown by dotted lines.

α. Fig. 8 shows a comparison of the stable results predicted by the beam and shell models. Although the values are in reasonable agreement, there is considerable disparity about when the solution exists. However, this solution, for both cases, is only just stable, and hence this disagreement is not unexpected, particularly for small α, where the boundary layer will be proportionally large. For both the beam and shell models, for large α, the results tend towards $R/a = 0.503$ and $\Phi R = -0.095$.

Fig. 9 shows the transverse cross-sectional shape, $w(y)$, for the shell model for $\alpha = 360°$. The cross-sectional shape from the beam model, where constant transverse curvature was assumed, is shown as a dotted line.

3.3. Isotropic case

For the isotropic case, the expressions for the torque and the longitudinal moment reduce to

$$T = 2lD\Phi\left(\left[a^2\Phi^2 + v - \frac{a}{R}\right]d_1 + (1 - v)\right), \tag{28}$$

$$M_l = -Dla\left[a\Phi^2 + \frac{v}{a} - \frac{1}{R}\right]^2 d_2 - Dl\left[a\Phi^2 + \frac{v}{a} - \frac{1}{R}\right]\left[\Phi^2 a^2 - v\right]d_1 + D\frac{l}{a}(1 - v^2), \tag{29}$$

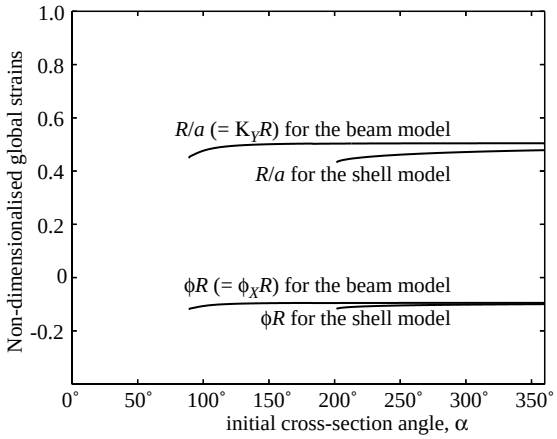

Fig. 8. A comparison of the prediction for the position of a second stable equilibrium configuration for the beam and shell models with a 40° symmetric layup.

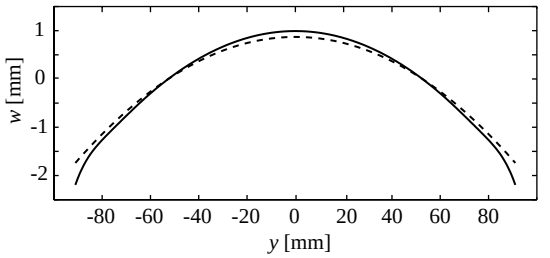

Fig. 9. Cross-sectional shape at the second stable equilibrium, for $\alpha = 360°$, for the 40° symmetric layup. The solid line is the prediction made by the shell model. The dashed lines is the prediction made by the beam model. The vertical scale is magnified 20 times compared with the horizontal scale.

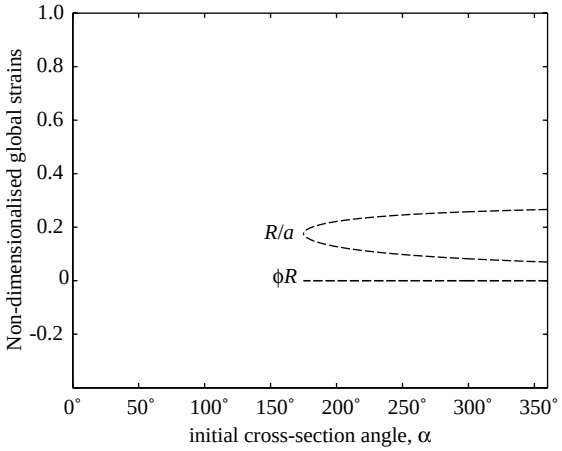

Fig. 10. Equilibrium points in addition to the initial state for the isotropic case. There are only unstable equilibria, which exist for $\alpha \geqslant 175°$, shown by dashed lines.

where v is the Poisson's ratio of the material and $D = Et^3/12(1 - v^2)$ is the bending stiffness: t is the thickness of the material, and E is the Young's modulus.

Solving these equations numerically shows that there are *no* stable solutions in this case. Fig. 10 shows how the values of the strains at the equilibrium point vary with the initial cross-sectional angle α. Unstable solutions appear for $\alpha \geqslant 175°$; for these solutions Φ_X is always zero. These solutions correspond to the stable/unstable pair of solutions for the 45° antisymmetric layup, but in this case both branches are unstable.

4. Comparison with experimental results

For the antisymmetric 45° layup, the predicted values given by the shell model for the longitudinal radius of curvature in the coiled state, a, can be compared with previous experimental and computational results. Table 1 updates the comparative table of results given in Part I to include the radius of curvature found using the shell model. It can be seen that the shell model is in particularly good agreement with the finite element calculations. The disparity with experiments is thought to be due to the inelastic nature of the matrix material used in the experiments, as discussed in Part I.

The finite element model used is described in detail by Iqbal (2001). It was generated using Abaqus (2002). A length of tube was modelled with a 48 by 48 mesh (24 by 24 for the $\alpha = 90°$ case) using S4R

Table 1
The coiled longitudinal radius of curvature, a, found using the shell model, compared with results from the beam model (Part I), experiments and finite element calculations, for the 45° antisymmetric layup with $R = 29$ mm

α (°)	Experiment (mm)	Beam model (mm)	Shell model (mm)	Finite element (mm)
280	30	38.5	40.0	39.6
200	30	38.5	40.7	40.5
120	32	38.7	42.7	43.0
90	33	39.2	45.1	45.7

The experimental results are from Iqbal et al. (2000) and are described in Part I.

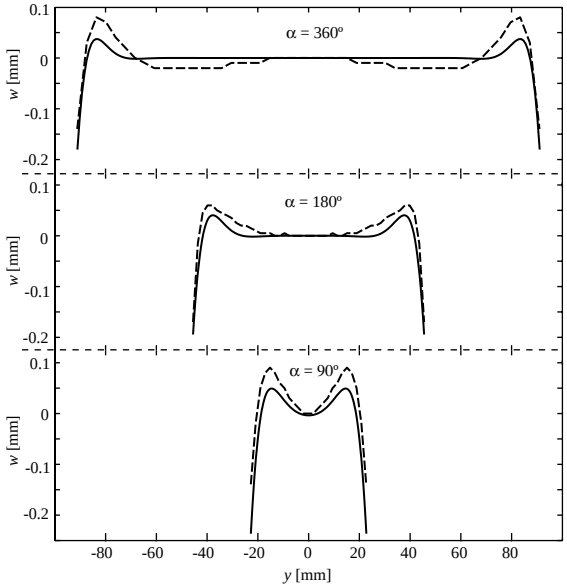

Fig. 11. Cross-sectional shape at the second stable equilibrium, for $\alpha = 90°$, 180°, and 360° for the 45° antisymmetric layup. The solid lines are the predictions made by the shell model. The dashed lines are the predictions made by the finite element model. The vertical scale is magnified 200 times compared with the horizontal scale.

elements, and geometrically non-linear elasticity. Edge moments were applied to flatten the original structure, and were then removed when close to the second stable equilibrium. Measurements were then taken from this state.

Fig. 11 shows a comparison of the cross-sectional shape predicted by the shell model, and by the finite element model, for $\alpha = 360°$, 180°, and 90°. For each case, both models reproduce essentially the same features: a flat central region with boundary layers at each edge, which are almost joined for the case $\alpha = 90°$.

5. Conclusions

This paper has shown that at a second equilibrium point for an antisymmetric bistable tube, a short 'boundary layer' will form at the edge of the tube, while the rest of the tube coils uniformly into a cylinder. For tubes that initially subtend a large cross-sectional angle, this effect is not important, but for tubes that initially subtend a small cross-sectional angle, the relatively large size of the boundary layer significantly affects the position, and even the existence, of a stable second equilibrium point.

Acknowledgements

We would like to thank RolaTube Technology Ltd., and particularly Andrew Daton-Lovett for help and support during this work. We would like to thank Sergio Pellegrino and Khuram Iqbal for many helpful discussions, and access to experimental and computational results. Diana Galletly was supported by a

studentship from the EPSRC. Simon Guest acknowledges support from the Leverhulme Trust, and Harvard University Division of Engineering and Applied Sciences.

References

Abaqus version 6.3, 2002. Hibbit, Karlsson & Sorenson, Inc., Pawtucket, RI, USA.
Calladine, C.R., 1983. Theory of Shell Structures. Cambridge University Press.
Eckold, G., 1994. Design and Manufacture of Composite Structures. Woodhead Publishing.
Galletly, D.A., 2001. Modelling the equilibrium and stability of slit tubes. PhD Thesis, University of Cambridge.
Galletly, D.A., Guest, S.D., 2004. Bistable composite slit tubes, I: A beam model. International Journal of Solids and Structures, this issue.
Iqbal, K., 2001. Mechanics of a bi-stable composite tube. PhD Thesis, University of Cambridge.
Iqbal, K., Pellegrino, S., Daton-Lovett, A., 2000. Bi-stable composite slit tubes. In: Proceedings of IUTAM-IASS Symposium on Deployable Structures. Kluwer.
James, G., 1996. Modern Engineering Mathematics. Addison Wesley Publishing Company.
Mansfield, E.H., 1973. Large-deflexion torsion and flexure of initially curved strips. Proceedings of the Royal Society A 334, 227–298.